

Directionally solidified calcia stabilised zirconia–nickel oxide plates in anode supported solid oxide fuel cells

R.I. Merino*, J.I. Peña, M.A. Laguna-Bercero, A. Larrea, V.M. Orera

Instituto de Ciencia de Materiales de Aragón, C.S.I.C.–Universidad de Zaragoza, Pedro Cerbuna 12, 50009 Zaragoza, Spain

Abstract

We present here a new manufacturing procedure for the anode Ni–zirconia cermet. It is based on the modification of the surface of a NiO–CaSZ (calcia stabilized zirconia) pellet of eutectic composition by surface laser melting and resolidification. A smooth, continuous and dense NiO–CaSZ layer is obtained on top of the ceramic pellet. Its depth can be varied from less than 200 μm to more than 570 μm , depending on the processing conditions. Its microstructure consists mainly of lamellar eutectic grains with interlamellar spacing ranging from 0.4 to 1.6 μm . The interspacing diminishes towards the surface, where a very fine microstructure is developed. Chemical reduction treatment transforms NiO to metallic Ni with the accompanying volume reduction. Complete reduction results into a cermet with 43 CaSZ + 33.5 Ni + 23.5 pores (%vol). Electrical conductivity is mainly electronic and proceeds along NiO lamellae or through percolating Ni particles.

© 2003 Elsevier Ltd. All rights reserved.

Keywords: Electrical conductivity; Fuel cells; Laser processing; ZrO_2

1. Introduction

The standard solid oxide fuel cells nowadays consist of YSZ as the electrolyte, a Ni–YSZ cermet as the anode and a mixed conducting oxide at the cathode.¹ The microstructure of the anode and anode–electrolyte interface is an important issue since it causes losses inside the operating cell. Sufficient porosity has to be provided in order to allow the fuel gas to reach the electrolyte surface, the metallic Ni load has to be enough to make the cermet electron conducting, and the particle size small in order to have a large triple phase boundary length.²

The fabrication procedures of the anode include the production of the component oxides in the form of fine powders, the homogenous mixing and the manufacturing of a ceramic pellet or tape with a controlled final density. Normally subsequent treatment in a reducing atmosphere transforms the NiO to Ni and increases the pore volume. Rarely the fabrication includes the melting of the oxides since they have high melting points and

this would cause a fast evolution of the microstructure, including grain growth.

Grain size control and processing by melting can be appropriately combined if a eutectic mixture is solidified. This is the approach we have undertaken here, to be more precise, we have used laser assisted directional resolidification at the surface of a pellet with the eutectic composition NiO–Calcia Stabilised Zirconia (CaSZ). The same procedure was previously used to fabricate dense plates of $\text{ZrO}_2\text{--Al}_2\text{O}_3$ ³ with good results: dense and homogeneous surface layers with thickness up to hundreds of microns. In the case of the CaSZ–NiO eutectic mixture grown by directional solidification,⁴ the microstructure consists of eutectic grains with a lamellar arrangement and well-bonded and coherent interfaces.⁵

Upon directional solidification of the upper surface on a ceramic substrate a gradient of interphase spacing and in alignment directions is expected from top to bottom.³ Subsequent chemical reduction to transform NiO to metallic Ni will produce the required porosity, necessary to make the cermet useful as an anode. In the present paper we will describe the preparation procedure of such composites and their resultant microstructure. Their electrical conductivity along the growth direction has been measured in air as well as in the reduced state.

* Corresponding author. Tel.: +34-976-761333; fax: +34-976-761229.

E-mail address: rmerino@posta.unizar.es (R.I. Merino).

2. Experimental procedure

Ceramic compacts of composition 25.5 mol% ZrO_2 + 4.5 mol% CaO + 70 mol% NiO were prepared. NiO (Aldrich 99.99%), ZrO_2 (Alfa 99%) and CaO (Aldrich 99.9%) powders were milled, calcined, mixed and pelletized. Afterwards they were sintered for 12 h at 1300 °C and 0.5 h at 1450 °C. Final densities were about 65%. The samples were processed on one side with laser light coming from different sources. For most of them we used a 600 W diode laser (approximately 810 nm) from Rofin Sinar. Others were processed with a Nd-YAG (1.06 nm) continuous wave laser from Spectron Laser Systems mod SL1101, with maximum power of 170 W. The conductivity measurements were done using a SOLARTRON 1260 impedance gain-phase analyser from Schlumberger Instruments (England). Scanning Electron Microscopy (SEM) micrographs and electron probe microanalysis (EPMA) were carried out with a JEOL 6400 microscope equipped with a Link Analytical eXL analyser.

The directional solidification was performed in the way sketched in Larrea et al.³ (Fig. 1). The samples were

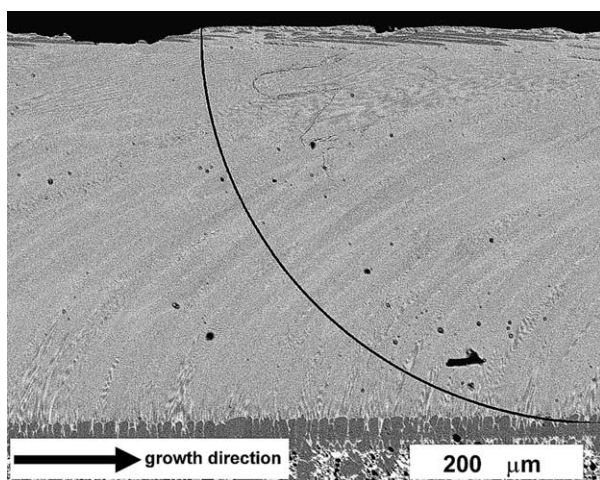


Fig. 1. SEM micrographs (back scattered electron image) of a longitudinal cross-section of laser melted $\text{ZrO}_2(\text{CaO})$ – NiO eutectics. The substrate ceramic is seen in the lower part of the picture. The bright phase is the $\text{ZrO}_2(\text{CaO})$ phase. The line indicates the approximate shape of the growth front.

located on top of Al_2O_3 large plates fixed to an automatic X-translator table. The light from the laser sources was handled optically in different ways to make it hit the sample from above as a thin focused line 10 mm long.

Reduction of the NiO to metallic Ni proceeds very fast⁶ (effective diffusion coefficient $\approx 2 \times 10^{-7} \text{ cm}^2\text{s}^{-1}$ at 850 °C). To achieve complete reduction and stable microstructure we annealed the samples for 3.5 h at 850 °C in 4% H_2 – N_2 .

3. Results and discussion

3.1. Microstructure of the plates: influence of the growth conditions

The microstructure of the laser-processed plates depends on the processing rate. After different trial experiments, we have chosen 500 mm/h as an appropriate travelling speed for the intended use as anodes. The treated depth ranged from 200 to 570 μm , depending on laser power. In Figs. 1 and 2 we show the microstructure of the samples processed at this rate. In Fig. 1 we can see a cross-section of the sample parallel to the X-stage travel direction (longitudinal cross-section). CaSZ is seen in the micrographs as the brighter phase and NiO as the darker one. A thin NiO layer nucleates first on top of the ceramic pellet (see Fig. 1); above it eutectic grains are formed. In the longitudinal section the eutectic grains bend to follow the thermal gradient. Details of these eutectic grains are better seen in Fig. 2. The eutectic microstructure is broken in the last 25 microns near to the outside surface. Primary NiO dendrites dominate surrounded by a very thin eutectic microstructure.

The formation of primary NiO dendrites and a thin NiO layer nucleating near to the ceramic can be due to deviations from the eutectic composition or to excessive undercooling at the used growth rate. We did not find in the literature information on the NiO – $\text{ZrO}_2(\text{CaO})$ phase diagram, apart from the works of Revcolevschi and its collaborators⁴ which report the eutectic composition. Moreover some evaporation is seen during the experiments, probably of NiO , which will in turn deviate the final composition from the nominal one.

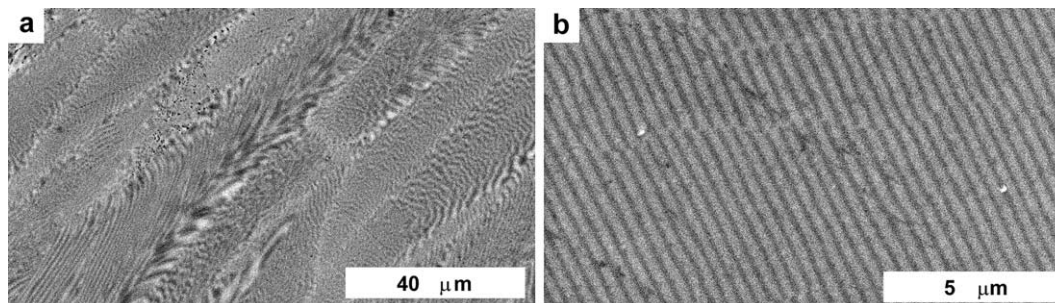


Fig. 2. (a) Longitudinal and (b) transverse cross-section details (longitudinal and transverse refer to the X-stage travel direction).

Microanalysis was performed in the largest dark and bright particles seen in the images. This shows that neither CaO nor ZrO_2 is dissolved into NiO. On the contrary, NiO is dissolved to a substantial amount into CaSZ, where about 6% atomic Ni compared to the total atomic metal content is found.

The lamellar morphology that dominates most of the volume of the processed sample is the one that was obtained previously by the floating zone method.^{7,4} The curved smooth shape of the advancing liquid–solid interface requires a gradient of solidification rates from top to bottom, which is associated with a gradient in interphase spacing. The interphase spacing (λ) normalised to the total processed depth is shown in Fig. 3 for two samples processed at 500 mm/h. They coincide nicely. λ ranges from 0.4 μm at the surface to 1.6 μm near to the unprocessed side of the NiO– ZrO_2 (CaO) pellet. Note the good agreement between the $\lambda = 0.4 \mu\text{m}$ at the surface, which corresponds to 500 mm/h growth rate, with the λ versus rate relationship reported by Revcolevschi et al.⁴

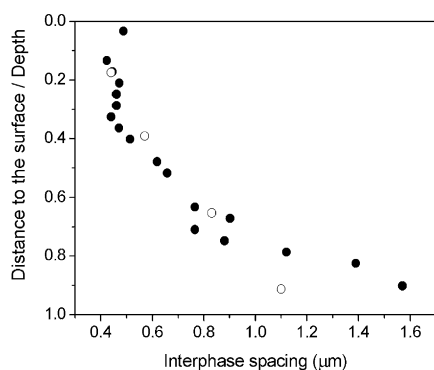


Fig. 3. Variation of the interphase spacing as a function of the distance to the outer surface for two samples treated with different power densities.

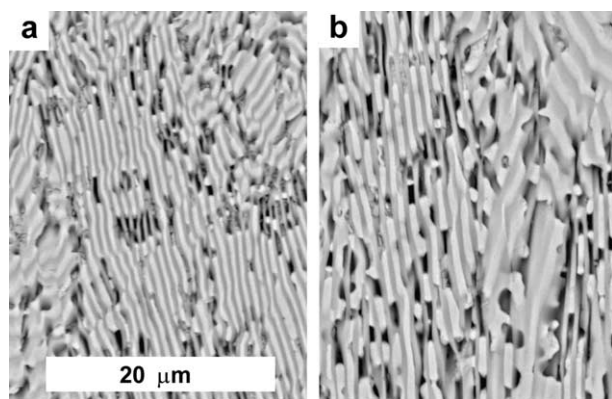


Fig. 4. SEM micrographs of transverse cross-sections of a sample reduced in 4% H_2 – N_2 at 850 $^\circ\text{C}$ at different depths (b is closer to the ceramic). The bright phase is the metallic Ni and the darkest zones correspond to pores.

3.2. Microstructure evaluation of the reduced samples: pore sizes and shapes

The resultant microstructure is shown in Fig. 4. These micrographs are taken on polished sections. Pores and Ni particles are sustained by the zirconia skeleton that serves as a mechanical support and as a barrier to stop the growth of the metallic Ni particles. The micrographs do not show the expected pore volume of 23.5%, which is the free space left when NiO reduces to metallic Ni, being the external sample dimensions fixed by the zirconia skeleton. In consequence, mesoporosity inside the Ni particles, and not observed in the SEM experiments, cannot be excluded. Nevertheless, a more or less homogeneous distribution of Ni particles and pores is formed, with accumulation of pores in sites where the lamellar microstructure shows imperfections. This provides a means to control the distribution of Ni and pores inside the cermet.

As expected from the original microstructure, the size of the Ni particles and of the pores grows from the outer surface (0.2 μm thick lamellae) to the interior of the sample. The 23.5% pore volume is perhaps insufficient to guarantee the absence of diffusion limitation polarisation in the anode. Whether this pore size and volume is appropriate to an anode supported fuel cell has to be checked by performing appropriate electrochemical characterisation. But two characteristics would favour its use. First that the zirconia skeleton, which occupies 43% of the total volume, supports the lamellar structure without cracking. Secondly, that the pore size, following the characteristic microstructural size, is graded from the top to the bottom of the structure, and consequently the triple phase boundary length will be maximum near to the upper surface, where the electrolyte can be attached.

3.3. Electrical conductivity

We separated the ceramic support from one of the processed samples by polishing it out and also slightly rectified the upper surface in order to eliminate the NiO dendrite region. We obtained a thin plate of 250 μm and with an approximate surface of $0.7 \times 0.8 \text{ cm}^2$. Four stripe electrical contacts were made with silver paste, such that the conductivity could be measured along the processing direction. A two-point configuration was used in the measurements in air or in a nitrogen flow. The frequency response showed a resistance independent of the frequency value at the lowest frequencies (1 Hz) that was taken as the resistance of the sample. We obtained its conductivity from this. The results are shown in Fig. 5. Values of conductivity of NiO in air and CaSZ taken from the literature are also shown for comparison (continuous lines). Since the conductivity of CaSZ does not change with oxygen partial pressure in

this P_{O_2} range, and is much smaller than the conductivity of the eutectic samples in either air or nitrogen, we can conclude that the latter is dominated by the conductivity of the NiO phase. From the plots, the average values of activation energies can be evaluated as 0.73 eV in air and 1.09 eV in nitrogen. The Arrhenius plots show a slight change of slope with temperature, also observed in measurements on laser floating zone grown samples, probably due to a change in the main mechanism of conductivity. We can conclude that conductivity is dominated by the NiO phase, whose lamellae must provide connected conducting paths along the sample. Similar values of conductivity are expected if conductivity was measured from top to bottom of the processed plate, since lamellae are oriented parallel to the growth direction and from the top to the bottom of the plate.

Park and Choi⁸ measured the conductivity of YSZ–NiO isotropic composites as a function of NiO content. Their results would give, for our composition, a mixed conducting character with a dominant NiO contribution to the total conductivity. Since our samples are preferentially aligned along the measurement direction and the conductivity of CaSZ is lower than that of YSZ, the electronic, NiO dominated range must have shifted to lower NiO contents, and thus NiO controlled conductivity in oxidising conditions is in agreement with those data.

After reduction the conductivity was measured using a four-point configuration. The results are also shown in Fig 5. The conduction is now metallic, with a smooth decrease in conductivity with temperature. If we compare the conductivity at room temperature with the metallic Ni conductivity we see that our cermet has, along the lamellae, a conductivity 50 times smaller than the one of bulk Ni. Conduction paths exist along the

metallic Nickel particles. A sufficient number of contact points must exist between Ni lamellae.

4. Conclusions

We have demonstrated the fabrication of dense composite plates of NiO–CaSZ with different thicknesses, performed by laser assisted surface melting and resolidification of ceramics with eutectic composition. The resultant microstructure is graded, with larger inter-lamellar spacing in the lower part of the sample and shorter nearer to the surface, which is smooth.

The structure is mechanically sustained when NiO is reduced to Ni + pore volume by the CaSZ skeleton. The resulting material is an electronic conductor. The small pore width in the upper side of the plate makes it possible to deposit a thin zirconia electrolyte dense layer. This work is in progress. The gradual variation of pore size from top to bottom of the structure and the possibility of controlling the pore sizes predict a good future for this approach to the preparation of solid oxide fuel cell anodes. The processing cost and scalability are not severe concerns, since large-scale equipment for laser surface materials processing is already being used industrially in other areas of materials processing. Some aspects related to minimising crack propagation have still to be addressed.

Acknowledgements

The work was financially supported by CICYT (Spain), under project MAT2000-1495.

References

1. Steele, B. C. H. and Heinzel, A., Materials for fuel-cell technologies. *Nature*, 2001, **414**, 345–352; Ivers-Tiffée, E., Weber, A., and Herbristrit, D., Materials and technologies for SOFC-components. *J. Eur. Ceram. Soc.*, 2001, **21**, 1805–1811; Huijsmans, J.P.P., Ceramics in solid oxide fuel cells. *Curr. Opin. Solid State Mat. Sci.*, 2001, **5**, 317–323.
2. Jiang, S. P., Callus, P. J. and Badwal, S. P. S., Fabrication and performance of Ni/3 mol% Y_2O_3 - ZrO_2 cermet anodes for solid oxide fuel cells. *Solid State Ionics*, 2000, **132**, 1–14.
3. Larrea, A., de la Fuente, G. F., Merino, R. I. and Orera, V. M., ZrO_2 - Al_2O_3 eutectic plates produced by laser zone melting. *J. Eur. Ceram. Soc.*, 2002, **22**, 191–198.
4. Dhalenne, G. and Revcolevschi, A., Directional solidification in the ZrO_2 system. *J. Cryst. Growth*, 1984, **69**, 616–618.
5. Dravid, V. P., Lyman, C. E., Notis, M. R., and Revcolevschi, A., Low energy interfaces in NiO– ZrO_2 (CaO) eutectic. *Metallurgical Transactions A*, 1990, **21**, 2309–2315; Dickey, E. C., Dravid, V.P. and Hubbard, C. R., Interlamellar residual stresses in single grains of NiO– ZrO_2 (cubic) directionally solidified eutectics. *J. Am. Ceram. Soc.* 1997, **80**, 2773–2780.

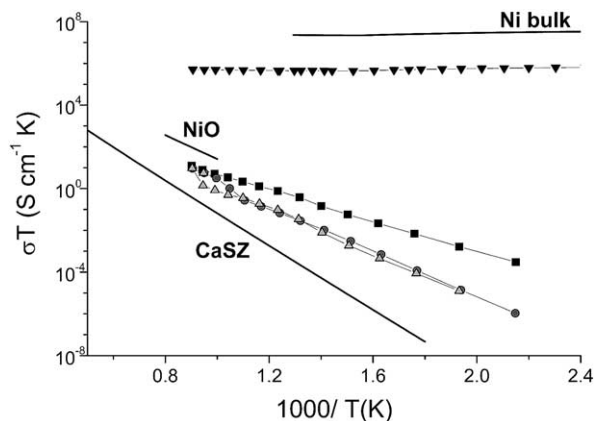


Fig. 5. Conductivity of oxidised and reduced states of ZrO_2 (CaO)–NiO plates along the growth direction as a function of temperature. ■ in air; ● and ▲ in dry nitrogen during down and up temperature runs respectively; ▼ in the reduced sample. Continuous lines depict data from the literature: Ni bulk,⁹ ZrO_2 (15 mol%CaO),¹⁰ and NiO¹¹.

6. Bonvalot-Dubois, B., Dhalenne, G., Berthon, J., Revcolevschi, A. and Rapp, R. A., Reduction of NiO platelets in a NiO/ZrO₂(CaO) directional composite. *J. Am. Ceram. Soc.*, 1988, **71**, 296–301.
7. Orera, V. M., Merino, R. I., Pardo, J. A., Larrea, A., Peña, J. I., González, C., Poza, P., Pastor, J. Y. and Llorca, J., Microstructure and physical properties of some oxide eutectic composites processed by directional solidification. *Acta Mater.*, 2000, **48**, 4683–4689.
8. Park, Y. M. and Choi, G. M., Mixed ionic and electronic conduction in YSZ-NiO composite. *J. Electrochem. Soc.*, 1999, **146**, 883–889.
9. Lutz, H., Scoboria, P., Crow, J. E. and Mihalisin, T., The effect of finite size on critical phenomena: the resistivity anomaly in Ni films. *Phys. Rev. B*, 1978, **18**, 3600–3611.
10. Orliukas, A., Bohac, P., Sasaki, K. and Gauckler, L. J., The relaxation dispersion of the ionic conductivity in cubic zirconias. *Solid State Ionics*, 1994, **72**, 35–38.
11. Mitoff, S. P., Electrical conductivity and thermodynamic equilibrium in nickel oxide. *J. Chem. Phys.*, 1961, **35**, 882–889.